RSC Advances

PAPER

View Article Online
View Journal | View Issue

Cite this: *RSC Adv.*, 2015, **5**, 31519

Controlled evaporative self-assembly of Fe_3O_4 nanoparticles assisted by an external magnetic field†

Yonghong Men,[ab] Wenqin Wang,*[a] Peng Xiao,[b] Jincui Gu,[b] Aihua Sun,[b] Youju Huang,[b] Jiawei Zhang*[b] and Tao Chen*[b]

Received 4th February 2015
Accepted 25th March 2015

DOI: 10.1039/c5ra02160j

www.rsc.org/advances

High fidelity and regularity structures of nanoscale materials has opened up new opportunities for developing miniaturized devices. A simple yet robust approach of magnetic field assisted controlled evaporative self-assembly (CESA) is developed to achieve Fe_3O_4 nanoparticle (NP) micro- and nano-patterns in a two dimensional (2D) direction. In the magnetic field assisted CESA process, the self-assembly morphology can be well controlled by varying extrinsic and intrinsic variables such as temperature, external magnetic field, and concentration of Fe_3O_4 NPs. Under the optimized magnetic field rotation frequency and temperature, 2D self-assembly of Fe_3O_4 NPs can be well realized. In addition, as photoactive sites, double bonds on the surface of Fe_3O_4 NPs allow the growth of polymer brushes by self-initiated photografting and photopolymerization (SIPGP), and the further achievement of free-standing magnetic composite films with well-defined patterns.

Introduction

High fidelity and regularity structures of nanoscale materials has opened up new opportunities for developing miniaturized electronic, opoelectronic, information-storage materials and devices, and biosensors.[1,2] In order to fabricate these ordered structures, several elegant methods have emerged, such as electrostatic self-assembly,[3] controlled anisotropic wetting/dewetting processes,[4] vertical convective self-assembly[5] or convective assembly in evaporative menisci,[6] evaporative-induced assembly,[7–9] evaporative lithography using a mask[10,11] and template-directed assembly.[12] Among these methods, evaporative-induced assembly has been recognized as an extremely simple, appealing strategy to achieve highly ordered, often intriguing structures. During the process of evaporative induced self-assembly of nonvolatile solutes (*e.g.*, polymers, nanoparticles, CNTs, and DNA) from a sessile drop, the flow instabilities, such as fingering instability and Marangoni flow often resulted in irregular dissipative structures (*e.g.*, randomly organized convection patterns, stochastically distributed multirings).[13,14] Recently, controlled evaporative self-assembly (CESA) in restricted geometries (*e.g.* two parallel plates with the top one sliding on the lower stationary substrate,[15] cylindrical geometry,[16] curve-on-flat geometries[7,17]) has allowed to form ordered yet complex structures or patterns. For instance, latex nanoparticles can be assembled into regularly arranged stripe patterns by subjecting a drop of polystyrene (PS) latex to evaporate from a liquid capillary bridge formed by confining the solution between a cylindrical lens and a Si substrate.[18] Besides, polymers, carbon nanotubes, graphene, DNA can also be organized into ordered yet complicated structures (*e.g.*, concentric rings,[7] snake-skin,[19] finger,[20] and spokes[21]) by CESA. During the process of solvent evaporation, external fields (*e.g.*, electric field) may promote the self-assembly of nonvolatile solutes. Velev reported that the application of electric field during convective assembly process increased the rate of colloidal crystal coating deposition and the size of crystal domains.[22]

As one of the most intensively studied magnetic materials,[23,24] magnetite (Fe_3O_4) has been showed great application potential in low-field magnetic separation, magnetic resonance imaging contrast agent, drug delivery, and mimetic enzymes because of their unique magnetic property.[25–27] Under the effect of external magnetic fields, magnetite or magnetic colloidal particles can be assembled into one-dimensional (1D) periodic chains,[28] 2D sheets,[29] 3D photonic crystals[30,31] or exciting and complex self-assembled structures.[2,32,33] For example, Gao *et al.* demonstrated a facile self-assembly of Fe_3O_4–SiO_2 beads into stable quasi-one-dimensional superstructures with the assistance of an external magnetic field.[34] Weddemann reported that highly ordered clusters and monolayers consisting of magnetic beads have been prepared by the employment of a rotating

[a]*Faculty of Materials Science and Chemical Engineering, Ningbo University, Ningbo 315211, China. E-mail: wqwang@126.com*

[b]*Division of Polymer and Composite Materials, Ningbo Institute of Material Technology and Engineering, Chinese Academy of Science, 1219 Zhongguan West Road, Ningbo 315201, China. E-mail: zhangjiawei@nimte.ac.cn; tao.chen@nimte.ac.cn*

† Electronic supplementary information (ESI) available: The SEM, optical, AFM images of Fe_3O_4 nanoparticles, Fe_3O_4 nanoparticles patterns and free-standing film. See DOI: 10.1039/c5ra02160j

magnetic field (*i.e.*, a magnetic stirrer RCT classic).[35] The alignment induced by an external magnetic field is highly preferable in several aspects, as this can be, noninvasive in nature, low cost, and relatively easy to be implemented. However, the alignment direction of magnetic nanoparticles is only parallel to the magnetic field and the regularity is not well. Therefore, the development of convenient methods to achieve the patterns of magnetic nanoparticles has attracted extensive attention in recent years and still remains a challenge.

Herein, we report a robust and scalable technique to fabricate Fe_3O_4 nanoparticles (NPs) patterns on Si substrate *via* CESA combining with an external magnetic field, and realize two-dimensional (2D) self-assembly (*i.e.*, the formation of linear stripes along magnetic field direction and concentric rings due to the confined geometry of sphere-on-flat) of Fe_3O_4 NPs. The effects of magnetic field rotation frequency, temperature and concentration of Fe_3O_4 solution on the formation of Fe_3O_4 NPs patterns were systematically explored. The optimization of magnetic field rotation frequency and temperature rendered 2D self-assembly of Fe_3O_4 NPs. Besides, as photoactive sites, double bonds on the surface of Fe_3O_4 NPs can be initiated to grow patterned polymer brushes by self-initiated photografting and photopolymerization (SIPGP) from Fe_3O_4 NPs patterns without a surface bonded initiator, and endowing the functionality of self-assembly patterns. This facile, robust method based on magnetic field assisted CESA offers a new avenue for patterning magnetic nanoparticles over large areas and achieving 2D self-assembly of magnetic nanoparticles.

Experimental section

Materials

The spherical lens made from fused silica (diameter 1 cm) and Si wafer were cleaned in the mixture of H_2O_2/H_2SO_4 (1 : 3, v/v) ("piranha solution") at 80 °C for 1 h and washed thoroughly with deionized water and blow-dried with N_2. Styrene (99%) was obtained from Alfa Aesar China (Tianjin) Co., Ltd, which was purified by neutral Al_2O_3 column chromatography and dried with 0.4 nm molecular sieve for 3 days at room temperature. 3-(trimethoxysilyl)propyl methacrylate (TMSPMA) was obtained from TCI.

Preparation of double bond modified Fe_3O_4 NPs[36]

Fe_3O_4 NPs were prepared according to previous report (Fig. S1†).[37] In a round bottom flask, Fe_3O_4 (0.5 g) and 3-(trimethoxysilyl)propyl methacrylate (TMSPMA) (0.3 mL) were dissolved in ethanol (45 mL) and stirred for 24 h at room temperature. Following, the solution was washed with ethanol by centrifugation (1600 rpm). Finally, Fe_3O_4 NPs were dried in the oven at 60 °C. As shown in Fig. S2,† absorption bands at 2920 cm^{-1} and 1628 cm^{-1} are attributed to stretching vibrations of $-CH_2$ and the vinyl groups of TMSPMA, respectively. The FTIR results confirm that TMSPMA was successfully grafted onto the Fe_3O_4 NPs *via* the silanization reaction. Fe_3O_4 solution (0.05, 0.1, and 0.2 mg mL^{-1}) was prepared by dissolving Fe_3O_4 NPs in the mixture solution of ethanol and deionized water (1 : 3, v/v) because of the poor dispersion of Fe_3O_4 NPs in deionized water.

Magnetic field assisted CESA of Fe_3O_4 NPs

The magnetic field used for the Fe_3O_4 NPs assembly is created by a magnetic stirrer RCT classic (IKA). The wafer was positioned in the center of the hot plate of the magnetic stirrer. A drop of Fe_3O_4 solution (10 μL) was loaded on Si wafer, then the spherical lens was brought into contact with Si substrate. The evaporation process was carried out at 50 °C and it took about 5 to 10 min.

SIPGP[38]

The patterned Si wafer was submerged in 2 mL of styrene and irradiated with an UV lamp with a spectrum between 300 and 400 nm (intensity maximum at $\lambda = 350$ nm with a total power of 9 mW cm^{-2}) for 1 h. Then, the substrate was exhaustively rinsed with different solvents (toluene, ethyl acetate, and ethanol) to remove physisorbed polymer and monomer.

Characterization

The 2D self-assembly patterns produced on Si substrate were characterized by optical microscopy (Olympus BX51) in the reflection mode and atomic force microscopy (CSPM 5500) in tapping mode. The spring constant of scanning probes is 40 N m^{-1}. Scanning electronic microscopy (SEM) measurements were carried out using a JEOL JMS-7600F scanning microscope. Fourier transform infrared (FTIR) spectrum was performed on a Varian Scimitar1000 Fourier transform IR spectrophotometer.

Results and discussion

Magnetic field assisted CESA is a convenient method to achieve 2D Fe_3O_4 NPs patterns. The process for achieving 2D self-assembly of Fe_3O_4 NPs *via* magnetic field assisted CESA is schematically shown in Fig. 1. Fe_3O_4 NPs with a diameter of 100 nm (Fig. S1†), were used as nonvolatile solute. According to our previous work,[39] if Fe_3O_4 NPs solution were limited in sphere-on-flat geometry (Fig. 1A), concentric rings could be

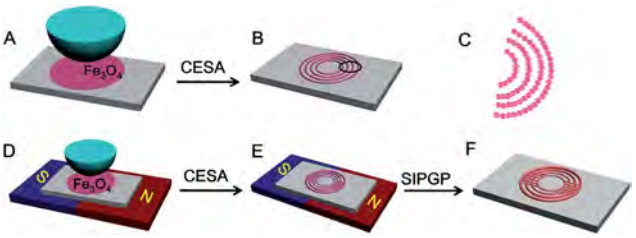

Fig. 1 Schematic procedure of CESA of Fe_3O_4 NPs without or with an external magnetic field. (A) CESA of Fe_3O_4 NPs in sphere-on-flat geometry. (B) Concentric rings of Fe_3O_4 NPs formed by CESA. (C) Schematic diagram self-assembly of Fe_3O_4 NPs marked in (B). (D) Magnetic field assisted CESA of Fe_3O_4 NPs in sphere-on-flat geometry. (E) Schematic diagram of 2D self-assembly of Fe_3O_4 NPs. (F) Growing polymer brushes by SIPGP from Fe_3O_4 NPs patterns.

formed (Fig. 1B and C). Due to the magnetic property of Fe_3O_4 NPs, an external magnetic field is employed to coordinate CESA of Fe_3O_4 NPs. First, a Si wafer was positioned in the center of a hot plate of a magnetic stirrer (IKA). Then, 0.1 mg mL^{-1} Fe_3O_4 NPs solution was loaded between a spherical lens and the Si substrate (Fig. 1D), evaporative loss of solvent at the capillary edge triggered the pinning of the solution/air/substrate three-phase contact line, thereby forming a coffee-ring deposit. During the process of evaporation, the initial contact angle of the capillary edge decreased gradually to a critical angle due to continuous evaporation of the solvent, at which the capillary force (depinning force) became larger than the pinning force. This caused the contact line to jump to a new position, and a new ring was developed. Consequently, the repetitive pinning and depinning cycles (*i.e.*, "stick-slip" motion) of the contact line led to the formation of concentric rings of Fe_3O_4 NPs.[7] In the presence of external magnetic field, Fe_3O_4 NPs would self-assemble along the magnetic field direction during the formation of concentric rings of Fe_3O_4 NPs. Therefore 2D self-assembly of Fe_3O_4 NPs can be achieved *via* the magnetic field assisted CESA (Fig. 1E). Finally, double bonds modified on the surface of Fe_3O_4 NPs were successfully initiated to grow patterned polymer brushes by SIPGP from Fe_3O_4 NPs patterns (Fig. 1F).

During the process of magnetic field assisted CESA, temperature plays an important role in the formation of concentric rings. On the one hand, the increase of temperature would lead to higher evaporation rate of solvent at the three-phase contact line, and thereby faster receding of the three-phase contact line, which in turn promotes the alignment of Fe_3O_4 NPs at the three-phase contact line. On the other hand, the increase of temperature would facilitate the convective flow that carries Fe_3O_4 NPs from the solution to the three-phase contact line, therefore more Fe_3O_4 NPs would deposit at the three-phase contact line.[7] For a static magnetic field ($f = 0$ rpm), it is conducive to form liner stripes along magnetic field direction (Fig. 2A). However, at relatively low temperature (*i.e.*, $T < 40$ °C), the evaporation rate is quite slow and concentric rings are almost not formed due to the insufficient radial flow to transport Fe_3O_4 NPs to the contact line (Fig. S3A†). At $T = 40$ °C, the regularity of patterns is reduced (Fig. 2B and S3B†), even though the formation of concentric rings is occurred. At $T = 60$ °C, the regularity of surface patterns (Fig. 2D and S3D†) is not well due to the increase fingering instabilities.[1,7] Therefore, $T = 50$ °C is identified as an optimal temperature, at which the meniscus receded neither too slow to cause only the formation of linear stripes along magnetic field direction and almost no concentric rings, nor too fast so that the regularity of patterns is broken (Fig. 2C and S3C†).

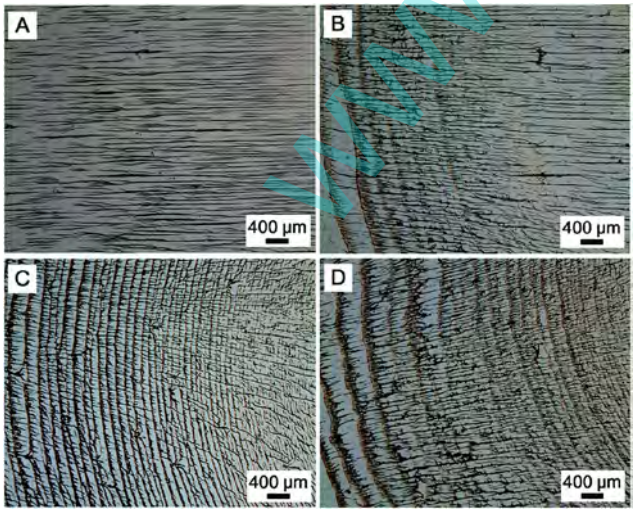

Fig. 2 Optical micrograph images of Fe_3O_4 NPs patterns under different temperatures (room temperature for A, 40 °C for B, 50 °C for C, 60 °C for D) with static magnetic field ($f = 0$ rpm).

In addition to temperature, magnetic field rotation frequency is also found to exert a profound influence on the 2D self-assembly of Fe_3O_4 NPs. As shown in Fig. 3, increasing magnetic field rotation frequency from 0 to 300 rpm, the phenomenon of the 2D self-assembly gradually disappears and finally there is only the formation of concentric rings. Small magnetic force is obtained if less magnetic particles are placed in a homogeneous magnetic field.[40] However, for sufficiently particle concentrations, if the magnetic field is stationary, the interaction between particles is very strong and the alignment of magnetic moment vectors entails an attractive force at stationary magnetic field, and both these resulted in the formation of 1D chain structures (Fig. 3E). The chain direction is only parallel to the magnetic field as long as viscous drag forces are small enough to be omitted. When the magnetic field is rotated at low magnetic field rotation frequency, the chain structures could also rotate (Fig. 3E). However, the chain rotation is damped by the viscosity of the carrier liquid, which exerts shear forces along the chain and leads to a phase lag, resulting in the chain direction not match with magnetic field direction.[41] Therefore, when magnetic field rotation frequency is small, the self-assembly of linear stripes along magnetic field direction is still occurred (Fig. 3A and B, S4A and S4B†). However, if the rotation frequency exceeds the critical rotation frequency, the viscous drag forces become too strong and the chains can no longer follow the rotation, and such chain structures cannot maintain their stability, resulting in the reorganization of Fe_3O_4 NPs in ordered 2D sheets (Fig. 3E).[40] However, due to the confined geometry (*i.e.*, sphere-on-flat), there is no formation of ordered 2D sheets and leading to only concentric rings when higher magnetic field rotation frequency is employed (Fig. 3C and D, S4C and S4D†). At the same time, the "stick-slip" motion of the contact line result that there are some Fe_3O_4 NPs between adjacent concentric rings (Fig. S4C and S4D†). Therefore, only when temperature is 50 °C and magnetic field rotation frequency is 0 rpm (static magnetic field), the 2D self-assembly behavior of magnetic field assisted CESA is the best.

Under the optimal temperature ($T = 50$ °C) and static magnetic field ($f = 0$ rpm), the influence of concentration on the process of magnetic field assisted CESA was investigated. As shown in Fig. 4, increasing the concentration of Fe_3O_4 NPs solution is not only advantageous to the self-assembly of linear stripes along magnetic field direction (Fig. 2C, 4A and C, S4A, S4C, and S4E†), but also to the formation of concentric rings

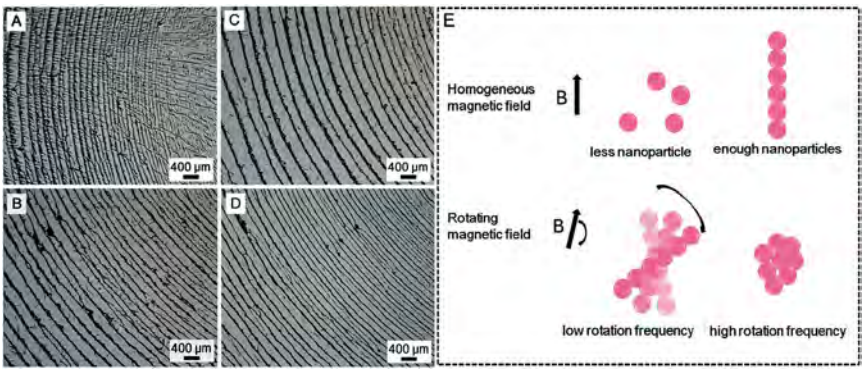

Fig. 3 Optical micrograph images of Fe_3O_4 NPs patterns with different magnetic field rotation frequency (0 rpm for A, 100 rpm for B, 200 rpm for C, 300 rpm for D) at 50 °C. (E) Schematic representation of the magnetic field induced assembly of magnetic particle.

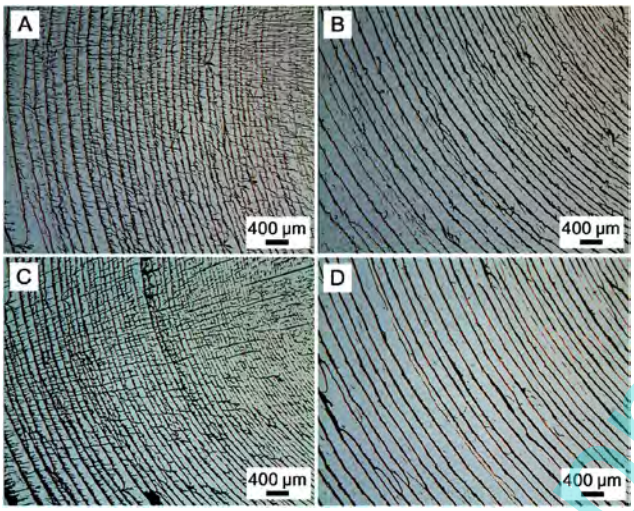

Fig. 4 Optical micrograph images of Fe_3O_4 NPs patterns with different concentrations (0.05 mg mL^{-1} for A and B, 0.2 mg mL^{-1} for C and D) under the optimal temperature ($T = 50$ °C) and static magnetic field ($f = 0$ rpm) (A and C, along magnetic field direction, B and D, perpendicular to magnetic field direction).

(Fig. S3C, 4B and D, S4B, S4D, and S4F). The higher concentration caused more deposition of Fe_3O_4 NPs from the solution to the three-phase contact line, corresponding to smaller critical angle.[17] Therefore, the pinning time of the contact line was longer, which lead to longer linear stripes along magnetic field direction. As shown in Fig. 2C, 4 and S5,† the length of linear stripes is changed from 25 μm to 40 μm, 85 μm corresponding to 0.05 mg mL^{-1}, 0.1 mg mL^{-1}, and 0.2 mg mL^{-1} of Fe_3O_4 NPs solution, respectively. The average width of ring is changed from 4 μm to 6 μm and 7 μm, and the average spacing of ring is changed from 45 μm to 37 μm and 27 μm, at the same time, the average width of the stripes is increased from 3 μm to 4 μm and 7 μm, corresponding to 0.05 mg mL^{-1}, 0.1 mg mL^{-1}, and 0.2 mg mL^{-1} of Fe_3O_4 NPs solution, respectively, according to AFM images (Fig. S5†). In addition, with increasing concentration of Fe_3O_4 NPs solution, the interaction between nanoparticles increases and results in better formation of linear stripes along magnetic field direction. Besides, as shown in Fig. S6,† accumulation of Fe_3O_4 NPs becomes more compact with increasing concentration of Fe_3O_4 NPs solution.

Very recently, patterned polymer brushes can be prepared without a surface bound initiator by SIPGP on photoactive patterned SAMs.[39,42–44] As photoactive sites, double bonds on the surface of Fe_3O_4 NPs were successfully initiated to grow poly(styrene) (PS) brushes by SIPGP from Fe_3O_4 NPs patterns. The height of Fe_3O_4 NPs rings generated from 0.05 mg mL^{-1} Fe_3O_4 solution is about 200 nm (Fig. S5B†). After SIPGP, a higher pattern of 230 nm is formed (Fig. S7A†). More recently, free-standing films have received continued interest due to their potential applications in microsensors or actuators.[38,45] The patterned PS brushes grafted on Fe_3O_4 NPs patterns could be further released from the silicon surface by immersing the substrate in KOH aqueous solution. The floating film is easily observed with naked eye (Fig. S7B†), followed by transferring it onto another silicon surface for optical and scanning electron microscope (SEM) measurements. The resulting free-standing

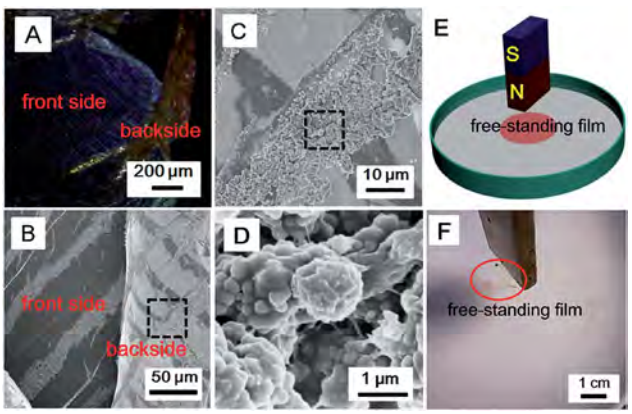

Fig. 5 Optical micrograph image and SEM images of free-standing film. (A) Optical image shows the front side and the backside of the free-standing film. (B) The SEM image including both the front side and the backside of the free-standing film. (C) The close-up SEM image marked in (B). (D) The close-up SEM image marked in (C). (E) The schematic plot of movement of free-standing film *via* a magnet. (F) The optical micrograph image of movement of free-standing film with a magnet.

composite film still has well-defined patterns (Fig. 5A). To scrutinize the surface morphology and the packing of Fe_3O_4 NPs, SEM measurements were performed. As shown in Fig. 5B and C, the patterns of Fe_3O_4 NPs are still observed from the free-standing film including both the front side and backside. Because of contacting with silicon surface, the spherical structure of Fe_3O_4 NPs is still retained on the backside of the free-standing film (Fig. 5D). However, the spherical structure on the front side of the free-standing film is not clearly seen because of the attached PS brushes (Fig. S7C and S7D†). In addition, the free-standing film can be moved with a magnet, which indicates the magnetic property of Fe_3O_4 NPs is not changed with PS brushes grafted on the surface (Fig. 5E and F and Movie S1†).

Conclusions

In summary, we demonstrated the two-dimensional self-assembly of Fe_3O_4 nanoparticles *via* magnetic field assisted controlled evaporative self-assembly. The self-assembly behavior could be tuned by temperature, magnetic field rotation frequency and the concentration of Fe_3O_4 nanoparticles solution. Besides, as photoactive template, patterned polymer brushes could be prepared *via* self-initiated photografting and photopolymerization on the surface of Fe_3O_4 nanoparticles. Furthermore, free-standing patterned polymer brushes film can be easily achieved and has magnetic property duo to the existence of Fe_3O_4 nanoparticles. The patterned polymer brushes and free-standing magnetic composite film may have potential applications in sensor devices and storage devices or other fields.

Acknowledgements

This research was supported by the Chinese Academy of Science for Hundred Talents Program, the Chinese Central Government for Thousand Young Talents Program, the National Natural Science Foundation of China (51303195, 21304105), Ningbo Natural Science Foundation (2014A610127), Ningbo Science and Technology Bureau (2014B81010) and Excellent Youth Foundation of Zhejiang Province of China (LR14B040001).

References

1 J. X. Huang, F. Kim, A. R. Tao, S. Connor and P. D. Yang, *Nat. Mater.*, 2005, **4**, 896–900.
2 R. M. Erb, H. S. Son, B. Samanta, V. M. Rotello and B. B. Yellen, *Nature*, 2009, **457**, 999–1002.
3 A. M. Kalsin, M. Fialkowski, M. Paszewski, S. K. Smoukov, K. J. M. Bishop and B. A. Grzybowski, *Science*, 2006, **312**, 420–424.
4 X. D. Chen, A. L. Rogach, D. V. Talapin, H. Fuchs and L. F. Chi, *J. Am. Chem. Soc.*, 2006, **128**, 9592–9593.
5 Y. Mino, S. Watanabe and M. T. Miyahara, *ACS Appl. Mater. Interfaces*, 2012, **4**, 3184–3190.
6 B. G. Prevo and O. D. Velev, *Langmuir*, 2004, **20**, 2099–2107.
7 J. Xu, J. F. Xia, S. W. Hong, Z. Q. Lin, F. Qiu and Y. L. Yang, *Phys. Rev. Lett.*, 2006, **96**, 066104.
8 Y. Lin, E. Balizan, L. A. Lee, Z. W. Niu and Q. Wang, *Angew. Chem., Int. Ed.*, 2010, **49**, 868–872.
9 L. Xiao, J. L. Wei, Y. Gao, D. G. Yang and H. M. Li, *ACS Appl. Mater. Interfaces*, 2012, **4**, 3811–3817.
10 D. J. Harris, H. Hu, J. C. Conrad and J. A. Lewis, *Phys. Rev. Lett.*, 2007, **98**, 148301.
11 D. J. Harris and J. A. Lewis, *Langmuir*, 2008, **24**, 3681–3685.
12 N. Meyerbroker and M. Zharnikov, *ACS Appl. Mater. Interfaces*, 2014, **6**, 14729–14735.
13 M. Maillard, L. Motte and M.-P. Poleni, *Adv. Mater.*, 2001, **13**, 200–204.
14 H. Hu and R. G. Larson, *J. Phys. Chem. B*, 2006, **110**, 7090–7094.
15 H. S. Kim, C. H. Lee, P. K. Sudeep, T. Emrick and A. J. Crosby, *Adv. Mater.*, 2010, **22**, 4600–4604.
16 M. Abkarian, J. Nunes and H. A. Stone, *J. Am. Chem. Soc.*, 2004, **126**, 5978–5979.
17 W. Han and Z. Q. Lin, *Angew. Chem., Int. Ed.*, 2012, **51**, 1534–1546.
18 W. Han, M. Byun and Z. Q. Lin, *J. Mater. Chem.*, 2011, **21**, 16968–16972.
19 M. Byun, R. L. Laskowski, M. He, F. Qiu, M. Jeffries-EL and Z. Q. Lin, *Soft Matter*, 2009, **5**, 1583–1586.
20 S. W. Hong, J. F. Xia, M. Byun, Q. Z. Zou and Z. Q. Lin, *Macromolecules*, 2007, **40**, 2831–2836.
21 B. Li, W. Han, M. Byun, L. Zhu, Q. Z. Zou and Z. Q. Lin, *ACS Nano*, 2013, **7**, 4326–4333.
22 J. Kleinert, S. Kim and O. D. Velev, *Langmuir*, 2010, **26**, 10380–10385.
23 G. Reiss and A. Hütten, *Nat. Mater.*, 2005, **4**, 725–726.
24 A. Weddemann, C. Albon, A. Auge, F. Wittbracht, P. Hedwig, D. Akemeier, K. Rott, D. Meissner, P. Jutzi and A. Hütten, *Biosens. Bioelectron.*, 2010, **26**, 1152–1163.
25 C. T. Yavuz, J. T. Mayo, W. W. Yu, A. Prakash, J. C. Falkner, S. Yean, L. Cong, H. J. Shipley, A. Kan, M. Tomson, D. Natelson and V. L. Colvin, *Science*, 2006, **314**, 964–967.
26 J. Q. Wan, W. Cai, X. X. Meng and E. Z. Liu, *Chem. Commun.*, 2007, **47**, 5004–5006.
27 K. Cheng, S. Peng, C. J. Xu and S. H. Sun, *J. Am. Chem. Soc.*, 2009, **131**, 10637–10644.
28 J. P. Ge, H. Lee, L. He, J. Kim, Z. D. Lu, H. Kim, J. Goebl, S. Kwon and Y. D. Yin, *J. Am. Chem. Soc.*, 2009, **131**, 15687–15694.
29 L. He, Y. X. Hu, H. Kim, J. P. Ge, S. Kwon and Y. D. Yin, *Nano Lett.*, 2010, **10**, 4708–4714.
30 T. Ding, K. Song, K. Clays and C.-H. Tung, *Adv. Mater.*, 2009, **21**, 1936–1940.
31 L. He, V. Malik, M. Wang, Y. X. Hu, F. E. Anson and Y. D. Yin, *Nanoscale*, 2012, **4**, 4438–4442.
32 L. Hu, R. R. Zhang and Q. W. Chen, *Nanoscale*, 2014, **6**, 14064–14105.
33 G. Singh, H. Chan, A. Baskin, E. Gelman, N. Repnin, P. Král and R. Klajn, *Science*, 2014, **345**, 1149–1153.
34 B. P. Jia and L. Gao, *Scr. Mater.*, 2007, **56**, 677–680.

35 A. Weddemann, F. Wittbracht, B. Eickenberg and A. Hütten, *Langmuir*, 2010, **26**, 19225–19229.
36 T. Y. Chen, Z. Cao, X. L. Guo, J. J. Nie, J. T. Xu, Z. Q. Fan and B. Y. Du, *Polymer*, 2011, **52**, 172–179.
37 J. F. Zhang, A. H. Sun, X. X. Qiao, C. Y. Chu, C. Y. Wang, T. Chen, J. J. Guo and G. J. Xu, *Mater. Res. Express*, 2014, **1**, 045037.
38 I. Amin, M. Steenackers, N. Zhang, A. Beyer, X. H. Zhang, T. Pirzer, T. Hugel, R. Jordan and A. Golzhauser, *Small*, 2010, **6**, 1623–1630.
39 Y. H. Men, P. Xiao, J. Chen, J. Fu, Y. J. Huang, J. W. Zhang, Z. C. Xie, W. Q. Wang and T. Chen, *Langmuir*, 2014, **30**, 4863–4867.
40 F. Wittbracht, B. Eickenberg, A. Weddemann and A. Hütten, *J. Appl. Phys.*, 2011, **109**, 114503.
41 I. Petousis, E. Homburg, R. Derks and A. Dietzel, *Lab Chip*, 2007, **7**, 1746–1751.
42 P. Xiao, J. C. Gu, J. Chen, D. Han, J. W. Zhang, H. T. Cao, R. B. Xing, Y. C. Han, W. Q. Wang and T. Chen, *Chem. Commun.*, 2013, **49**, 11167–11169.
43 P. Xiao, J. C. Gu, J. Chen, J. W. Zhang, R. B. Xing, Y. C. Han, J. Fu, W. Q. Wang and T. Chen, *Chem. Commun.*, 2014, **50**, 7103–7106.
44 M. Steenackers, S. Q. Lud, M. Niedermeier, P. Bruno, D. M. Gruen, P. Feulner, M. Stutzmann, J. A. Garrido and R. Jordan, *J. Am. Chem. Soc.*, 2007, **129**, 15655–15661.
45 I. Amin, M. Steenackers, N. Zhang, R. Schubel, A. Beyer, A. Golzhauser and R. Jordan, *Small*, 2011, **7**, 683–687.